



PAPER

Plasmon-modulated photoluminescence enhancement in hybrid plasmonic nano-antennas

OPEN ACCESS

RECEIVED
8 April 2020REVISED
23 July 2020ACCEPTED FOR PUBLICATION
14 August 2020PUBLISHED
11 September 2020

Original content from
this work may be used
under the terms of the
[Creative Commons
Attribution 4.0 licence](#).

Any further distribution
of this work must
maintain attribution to
the author(s) and the
title of the work, journal
citation and DOI.

Alireza R Rashed¹ , Mohsin Habib¹ , Nekhel Das¹, Ekmel Ozbay² and
Humeyra Caglayan^{1,3} ¹ Faculty of Engineering and Natural Sciences, Photonics, Tampere University, 33720 Tampere, Finland² NANOTAM-Nanotechnology Research Center, Bilkent University, 06800, Ankara, Turkey³ Author to whom any correspondence should be addressed.E-mail: humeyra.caglayan@tuni.fi and alireza.rashed@tuni.fi**Keywords:** plasmon, nano-antennas, photoluminescence, particle plasmons, hybrid exciton-plasmon systemSupplementary material for this article is available [online](#)

Abstract

In this work, we performed a systematic study on a hybrid plasmonic system to elucidate a new insight into the mechanisms governing the fluorescent enhancement process. Our lithographically defined plasmonic nanodisks with various diameters act as receiver and transmitter nano-antennas to outcouple efficiently the photoluminescence of the coupled dye molecules. We show that the enhancement of the spontaneous emission rate arises from the superposition of three principal phenomena: (i) metal enhanced fluorescence, (ii) metal enhanced excitation and (iii) plasmon-modulated photoluminescence of the photoexcited nanostructures. Overall, the observed enhanced emission is attributed to the bi-directional near-field coupling of the fluorescent dye molecules to the localized plasmonic field of nano-antennas. We identify the role of exciton–plasmon coupling in the recombination rate of the sp-band electrons with d-band holes, resulting in the generation of particle plasmons. According to our comprehensive experimental analyses, the mismatch between the enhanced emission and the emission spectrum of the uncoupled dye molecules is attributed to the plasmon-modulated photoluminescence of the photoexcited hybrid plasmonic system.

1. Introduction

The control over the spontaneous emission rate of a single quantum emitter (QE) has attracted particular interest, since it provides a powerful multifunctional tool for different promising applications [1–5]. During the last two decades, rapid advances in the field of nano-plasmonics have opened avenues for extremely high energy confinement below the diffraction limit [6]. The interaction of the localized surface plasmons (LSPs) with different types of quantum emitters (QEs) has stimulated the field of plasmon-enhanced spectroscopy [7–10].

In a quantum system, the electrons promoted to the excited state can relax back to the ground state via radiative or non-radiative decay channels. Depending on the design of a hybrid system, the competition between radiative and non-radiative decay rates results in either photoluminescence (PL) quenching or enhancement process [11–14]. In an engineered hybrid plasmonic system, the near-field coupling of an excitonic element to the enhanced local field of the plasmonic nano-antenna may speed up the radiative decay rate [15–18]. This can be achieved by overlapping the LSP mode of a plasmonic cavity with resonating mode of a QE, which is oscillating at the same polarization of the plasmonic cavity [19–21]. According to Fermi's golden rule, the photonic density of states (PDOS) of a plasmonic cavity can modify the spontaneous emission of a QE, known as the Purcell effect [22–24]. The Purcell factor can be significant for nano-resonators which have a high-quality factor and provide considerable local field confinement [24]. However, the stronger confinement implies stronger plasmonic losses. Therefore, in the design of an

efficient hybrid system, an optimized trade-off between these two effects should be considered. Such optimization can be done by changing the shape, size, composition and arrangement of the nano-resonators.

Besides exploiting radiative decay rate enhancement, one can manipulate the excitation rate of the QEs to achieve more significant spontaneous emission enhancement in hybrid systems [25–27]. Similar to radiative decay rate enhancement, excitation rate enhancement is strongly dependent on the orientation of QEs' dipoles relative to the resonance mode of the nano-resonator. Urena *et al* show that the PL signal of a coupled quantum dot to the monomers and dimers of gold nano-antennas is influenced by the separate modifications of the excitation rate and the quantum yield of the hybrid systems [28]. Similarly, in another work, the authors have optimized a hybrid system, consisting of gold nano-prism antennas and CdSe/ZnS nanocrystals to increase the excitation and/or emission rates of quantum dots, resulting in a significant enhancement of their fluorescence [29].

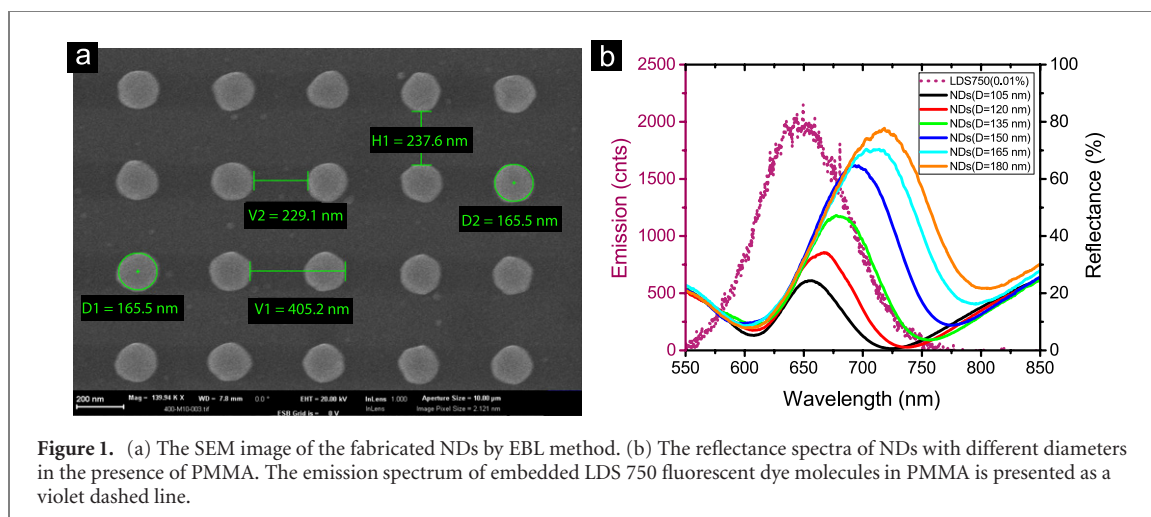
Even though the interaction between excitonic and plasmonic elements has been extensively studied in the last years, all underlying mechanisms related to the fluorescence enhancement process are not yet completely revealed. A hybrid system can be designed in such a way that in addition to the radiative decay rate enhancement and/or excitation rate enhancement, another process related to the radiative decay of particle plasmons (PPs) can contribute in the emission enhancement process.

The photoluminescence from noble metals has been reported in several earlier studies [30–33]. Through interband transitions, excitation photons of a light source with proper energy can establish non-equilibrium populations of electrons and holes in metal. The recombination of non-equilibrium populations of electrons and holes, located below and above Fermi level, can form highly localized electron–hole dipoles, leading to the polarization of the nanostructure and subsequently, the establishment of a coherent oscillation of the free electrons (PPs generation). In some studies, due to the enhanced local field around nano-antennas, some of the d-band holes undergo direct radiative recombination with electrons in the sp-band, leading to photoluminescence from the excited metals [32–35]. However, some other theoretical studies and experimental findings show that the observed PL from the photoexcited metallic structures originates from the radiative decay of the generated PPs which is associated with emitted photons [36–39]. In the experimental study of Hu *et al*, the observed PL of the photoexcited Au nanodisks (NDs) is attributed to the radiative decay of bright plasmon resonance modes [39]. They have shown the correlation between the LSP band and the acquired PL spectrum of the excited nanostructures. According to their observations, the PL intensity is depended on energy matching between excitation laser wavelength (532 nm, 2.33 eV) and plasmon resonance. Similar to this reported observation, in some studies on plasmonic hybrid systems, it is shown that the enhanced PL spectra of QEs closely tracks the LSP band of the nano-resonators [40–43]. However, to the best of our knowledge, the contribution of the plasmon-modulated PL in the enhanced emission of hybrid exciton–plasmon systems is overlooked.

The goal of this study is to realize a plasmonic hybrid system, consisting of the plasmonic nano-antennas and fluorescent dye molecules to reveal the underlying mechanisms behind the photoluminescence enhancement process. Our approach for modulating the spectral overlap between emission spectrum of the QEs and resonance band of the nano-antennas relies on modifying the diameter of NDs. We use steady-state fluorescence spectroscopy, as well as fluorescence lifetime imaging and spectroscopy methods to manifest increase of the spontaneous emission rate, as signatures of a bidirectional near-field coupling. The precisely engineered hybrid exciton–plasmon systems provide us the opportunity to exploit the enhanced local field of the nano-antennas by intensifying both excitation and spontaneous radiative decay rates. This is achieved by creating a simultaneous spectral overlap between the plasmon band of Au NDs and the emission and absorption spectra of LDS 750 fluorescent dye molecules. The photoexcited dye molecules, operating as radiating antennas, and the recombination of the photoexcited electrons in sp-band with d-band holes function as two pathways to induce plasmonic oscillation on NDs. We show that the radiative de-excitation of the generated PPs functions as an extra channel to enhance the radiative decay rate of the hybrid system. The contribution of the amplified plasmon-modulated photoluminescence in the enhanced emission of the hybrid system is manifested by the spectral shift of the enhanced emission with respect to the emission of the uncoupled dye molecules. Our results reveal the role of the bright-mode PPs in the PL enhancement process, leading to a new perspective in the engineering procedure of plasmonic hybrid systems for both fundamental science and technological applications.

2. Simulation and experimental results

We designed periodic arrays of plasmonic NDs with height of 70 nm and varied diameters from 105 to 180 nm, while keeping the period fixed as 400 nm. Figure 1(a) shows a scanning electron microscopy (SEM) image of the NDs, fabricated by standard electron-beam lithography (EBL) method on Si/SiO₂



substrate (for details see methods section). Figures S1(a) and (c) depict the simulated reflectance spectra of NDs with different diameters. The experimentally acquired reflectance spectra of the corresponding NDs are presented in figure S1(b). The comparison of the simulation and experimental results shows an excellent agreement between the design and fabrication. As the diameter increases, the strengthening and red-shift of the reflectance bands are evident in these results. The spectral shift in the resonance band of NDs with different diameters provides the opportunity to investigate the modification of the coupling efficiency between QEs and the local field of the designed nano-antennas.

In this work, we considered LDS 750 dye molecules as an appropriate QE. The fluorescent molecules with mass percent concentration of 0.01% are dissolved mono-dispersively and homogeneously in PMMA A2. For such concentration, the number of LDS 750 dye molecules located on the considered unit square area of PMMA host medium is calculated (see supplementary material (<https://stacks.iop.org/NJP/22/093033/mmedia>), section 3 and 4, for further details). The emission spectrum of the embedded LDS 750 dye molecules in PMMA is presented in figure 1(b), which is about 50 nm blue-shifted with respect to the case when they are dissolved in a polar solution [44]. One can explain the observed blue-shift according to photochemical properties of LDS 750 molecule. In the chemical structure of this hemicyanine dye, a dimethylamine group is linked to an aromatic ring (naphtha-thiazole) through an ethylene group. Due to the internal concomitant twisting motion of dimethylamine group, the formation of the twisted intramolecular charge transfer (TICT) state is the major deactivation pathway for the populated excited state. However, transition to the TICT state is strongly dependent on the viscosity and polarity of the surrounding medium [45]. In polar solvents such as ethanol and methanol, the emission originates from the TICT state rather than the locally excited state, resulting in a red-shifted emission spectrum. However, for LDS 750 molecules embedded in a rigid PMMA matrix, the emission is generated only from high-energy locally excited states. This occurs due to the hindering of large-amplitude motion, preventing the formation of TICT state, which is the relaxed state. Subsequently, transition of the excited electrons to the ground state through locally excited states results in a large blue-shift in the emission spectrum.

The measured reflectance spectra of the NDs with spin-coated PMMA is presented in figure 1(b). The presence of PMMA on NDs modifies the intensity, quality factor and spectral position of the plasmonic resonance, as compared to the case that the NDs are exposed to air (figure S1(b)). This occurs due to the change in the surrounding refractive index of NDs from air to PMMA ($n = 1.48$) [46]. The simulated reflectance spectra of NDs with PMMA layer is presented in figure S1(d). The obtained results are consistent with the acquired experimental results, confirming the role of PMMA layer in modifying the optical properties of the plasmonic nano-antennas. Furthermore, the local electric field intensity of NDs are calculated in the absence and the presence of PMMA layer (figure S2). Intensification of NDs local field in the presence of PMMA is evident in these results, leading to improve the strength of exciton-plasmon coupling in the designed hybrid system.

Figure 2(a) reports the enhanced PL of LDS 750 dye molecules in the presence of plasmonic NDs with different diameters. The observed increase in the emission intensity of the fluorescent dye molecules can be interpreted as the Purcell factor enhancement, as a result of the near-field coupling between the photoexcited QEs and plasmonic nano-resonators. However, as is discussed below, the other mechanisms contribute to the emission enhancement process. The spontaneous emission rate enhancement is correlated with the spatial overlap between fluorescent material and the plasmonic nano-antenna. In other words, the presence of the thin approximately 40 nm gain layer on top of NDs satisfies the desired condition for an

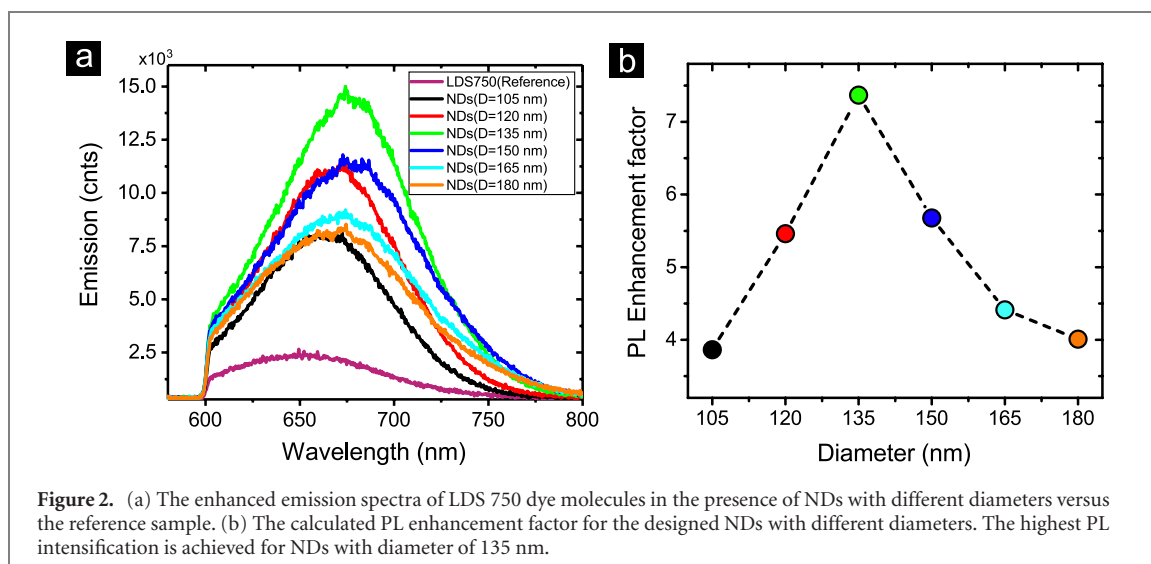


Figure 2. (a) The enhanced emission spectra of LDS 750 dye molecules in the presence of NDs with different diameters versus the reference sample. (b) The calculated PL enhancement factor for the designed NDs with different diameters. The highest PL intensification is achieved for NDs with diameter of 135 nm.

efficient interaction between dye molecules and the local fields of NDs. However, to avoid the possible self-quenching effect resulting from the direct charge transfer, a smooth 5 nm thick layer of Al_2O_3 is placed as a spacer between the active PMMA layer and NDs.

Additionally, the spectral overlap between the emission spectrum of fluorescent material and the extinction of plasmonic nanostructure is critical to accomplish an efficient emission enhancement. In the fluorescence enhancement process, both absorption and reflection properties of a nano-antenna play role. The absorbance of a nano-antenna corresponds to the absorptive losses (dark modes) and shows the interaction ability of the resonator with the incident light. On the other hand, the reflectance of a nano-antenna shows the capability of the resonator to out-couple the confined local field (bright modes) to the far-field. The reflectance band of the fabricated NDs on the non-transparent substrate of Si/SiO₂ is a signature for the spectral position of the localized surface plasmon resonance (LSPR) band of the nano-resonators (supplementary material, figure S3). By tuning the diameter of NDs, one can achieve a desired spectral matching between the LSP resonance band of the nano-resonators and the emission spectrum of LDS 750 dye molecules. We studied this for the PL enhancement in hybrid systems that consist of LDS 750 dye molecules and NDs with different diameters, changing from 105 nm to 180 nm with 15 nm step. The samples are excited far from the NDs resonance band by a continuous wave laser, operating at 532 nm. For each sample the PL enhancement factor is calculated as the ratio between LDS 750 photoluminescence in the presence and absence of nano-antennas. As is seen in figure 2(b), the maximum PL enhancement (7 folds) is achieved for NDs with diameter 135 nm, which has the best spectral overlap of the reflectance with the emission spectrum of the fluorescent molecules.

Figure 3(a) presents the power-dependent emission peak intensity of LDS 750 dye molecules in the presence and absence of NDs with diameter of 135 nm. It reveals the significant difference in the slope of the fluorescence count-rates, while the excitation power intensity is altered. The observed slope change clarifies that the coupling efficiency between the excited gain material and nano-antennas enhances, as the intensity of the excitation power increases. Indeed, a greater number of the excited gain dipoles can induce stronger dipolar LSPs and higher-order oscillations in NDs. Furthermore, as it will be discussed later, the utilized excitation source with the energy of 2.33 eV can induce plasmon oscillation in the nano-resonators. The higher intensities of the excitation source may lead to induce stronger plasmonic resonances in NDs. Therefore, the circumstance for the occurrence of stronger gain-plasmon interactions at higher excitation power intensities can be satisfied, leading to higher PL enhancement rates.

Subsequently, the fluorescent lifetime of LDS 750 dye molecules is measured for the designed hybrid exciton-plasmon systems. The shortening of the decay rates provides a signature for the near-field interactions between LDS 750 dye molecules and the plasmonic field of NDs (figure 3(b)). The acquired time-resolved fluorescence decay curves of the designed hybrid samples, including dye molecules embedded in PMMA, which all are fitted with a bi-exponential decay function, are presented in table 1. It is worth noting that according to our experimental observations, the kinetics of LDS 750 molecules dissolved in ethanol can be fitted with single exponential decay, resulting in the measured lifetime of 365 ps. However, in a rigid environment like PMMA, the large-amplitude motion of the excited molecules can be completely blocked. Moreover, intermolecular beatings as an extra non-radiative relaxation pathway are hindered in such rigid matrix. Therefore, in addition to the spectral shift of the emitted photons, the excited state

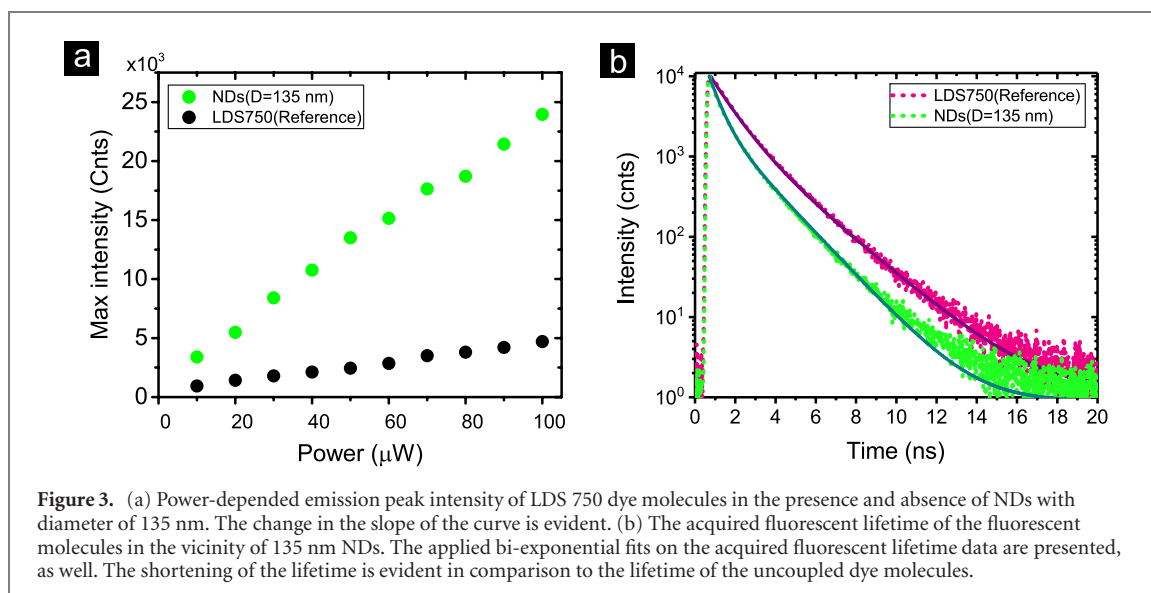


Figure 3. (a) Power-dependent emission peak intensity of LDS 750 dye molecules in the presence and absence of NDs with diameter of 135 nm. The change in the slope of the curve is evident. (b) The acquired fluorescent lifetime of the fluorescent molecules in the vicinity of 135 nm NDs. The applied bi-exponential fits on the acquired fluorescent lifetime data are presented, as well. The shortening of the lifetime is evident in comparison to the lifetime of the uncoupled dye molecules.

Table 1. Time-resolved fluorescence spectroscopy results for hybrid plasmonic systems with different diameters. τ_{Short} and τ_{Long} are the components of the bi-exponential function used to fit kinetics of embedded LDS 750 molecules in PMMA as well as hybrid systems.

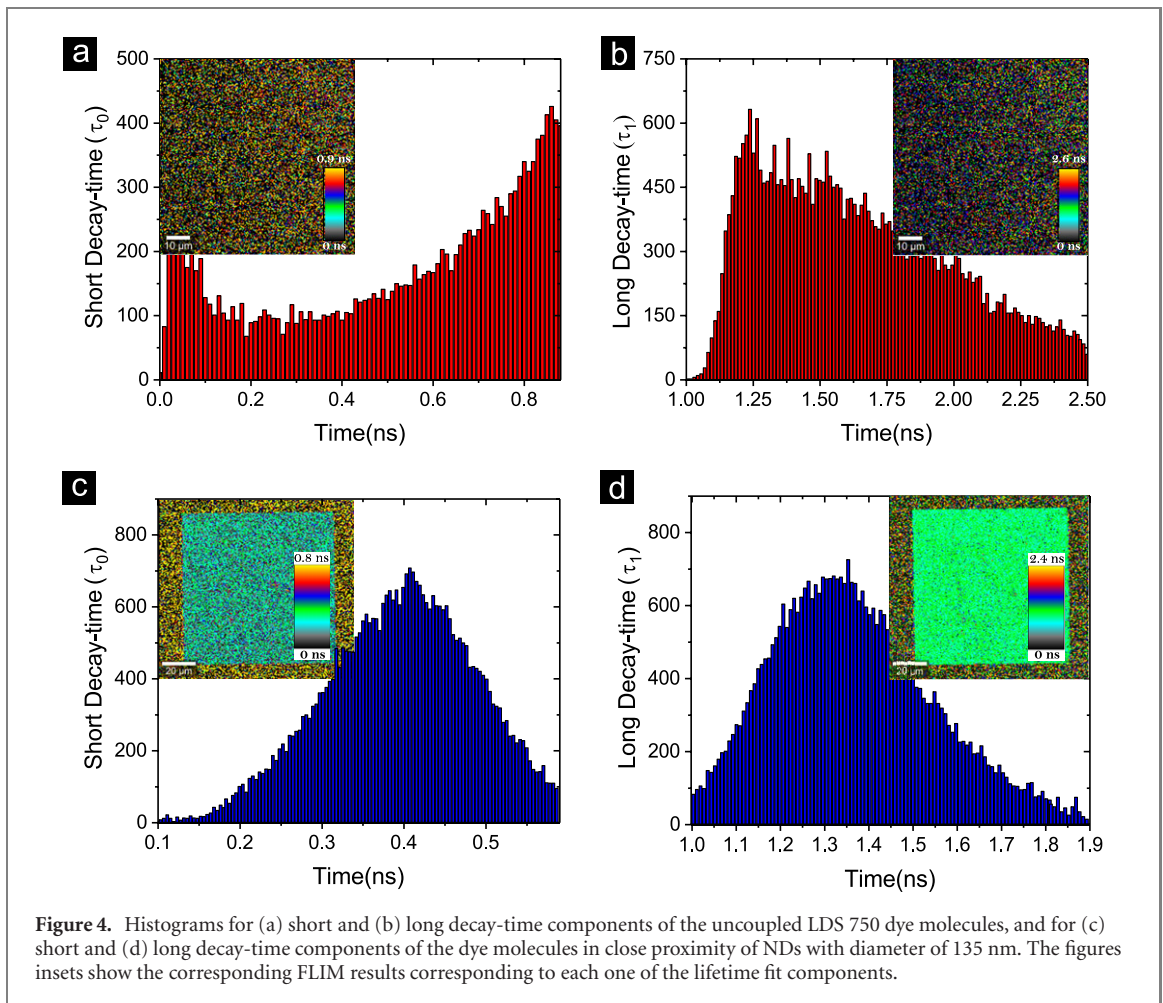
	LDS 750	105 nm	120 nm	135 nm	150 nm	165 nm	180 nm
τ_{Short} (ns)	1	0.49	0.46	0.45	0.52	0.56	0.59
τ_{Long} (ns)	2.09	1.69	1.67	1.66	1.67	1.68	1.71

lifetimes of LDS 750 dye are influenced by the viscosity and rigidity of the environment. This leads a longer average fluorescent lifetime in PMMA than that in ethanol [47]. Moreover, in such a dense matrix, the monomers of dye molecules may aggregate, providing two fluorescent lifetime components rather than the one component which is observed for dissolved LDS dye molecules in ethanol. The shortening of both short and long components in the measured decay times is obvious for all samples, in comparison to the reference sample (embedded LDS 750 molecules in PMMA far from NDs). Evidently, the change in the decay rates of the coupled LDS 750 to NDs with diameter of 135 nm is much more pronounced as compared to other NDs. Indeed, as a crucial factor to achieve much more efficient exciton–plasmon interaction, the highest spectral overlap is realized for this sample.

To provide a much clearer picture of the decay rates modification related to LDS 750 dye molecules, we have performed fluorescence lifetime imaging microscopy (FLIM). In figure 4 insets, we report the processed FLIM images related to the decay time fit components of the dye molecules, placed far from ((a) and (b)) and in the close vicinity ((c) and (d)) of the NDs with diameter of 135 nm. In these images, the spots with bright colors represent short lifetime components, while dark spots stand for the long lifetime components. The presence of the brighter colors, as a footprint for the shortened lifetimes, in both fast and slow decay fit components of the hybrid systems are evident. Moreover, to provide a quantitative presentation for the acquired lifetime fit components, the corresponding histograms of the acquired FLIM images are reported in figure 4. The shorter lifetimes (faster decay rates) can be noticed in the histograms of the coupled dye molecules.

3. Theory and discussion

Modifying the diameter allowed us to tune the spectral overlap between the LSPR band of NDs and the emission spectra of LDS 750 fluorescent dye molecules. We show that there is a correlation between the efficiency of the spectral overlap and PL enhancement rate. In addition, we engineered our plasmonic hybrid system in such a way that both emission and absorption bands of the used QEs overlap simultaneously with the nano-antennas LSP resonance band. This fact is depicted in figure 5(a), for NDs with diameter of 135 nm. Such spectral overlap influences the underlying mechanisms behind the enhanced PL of the coupled dye molecules to nano-antennas. In principle, three mechanisms are involved in the spontaneous emission enhancement process of our plasmonic hybrid systems: (i) Purcell effect



enhancement, (ii) excitation rate enhancement, and (iii) radiative decay of the photoexcited PPs. Depending on the physical circumstances, the contribution of each one of these three mechanisms in the overall enhanced emission can be differed. These mechanisms are illustrated as a scheme in figure 5(b). In general, the spontaneous emission rate (K_{em}) of a QE depends on the quantum yield (Φ_{QE}) and the excitation rate (K_{exc}) of that emitter.

$$K_{em} = \Phi_{QE}K_{exc}. \quad (1)$$

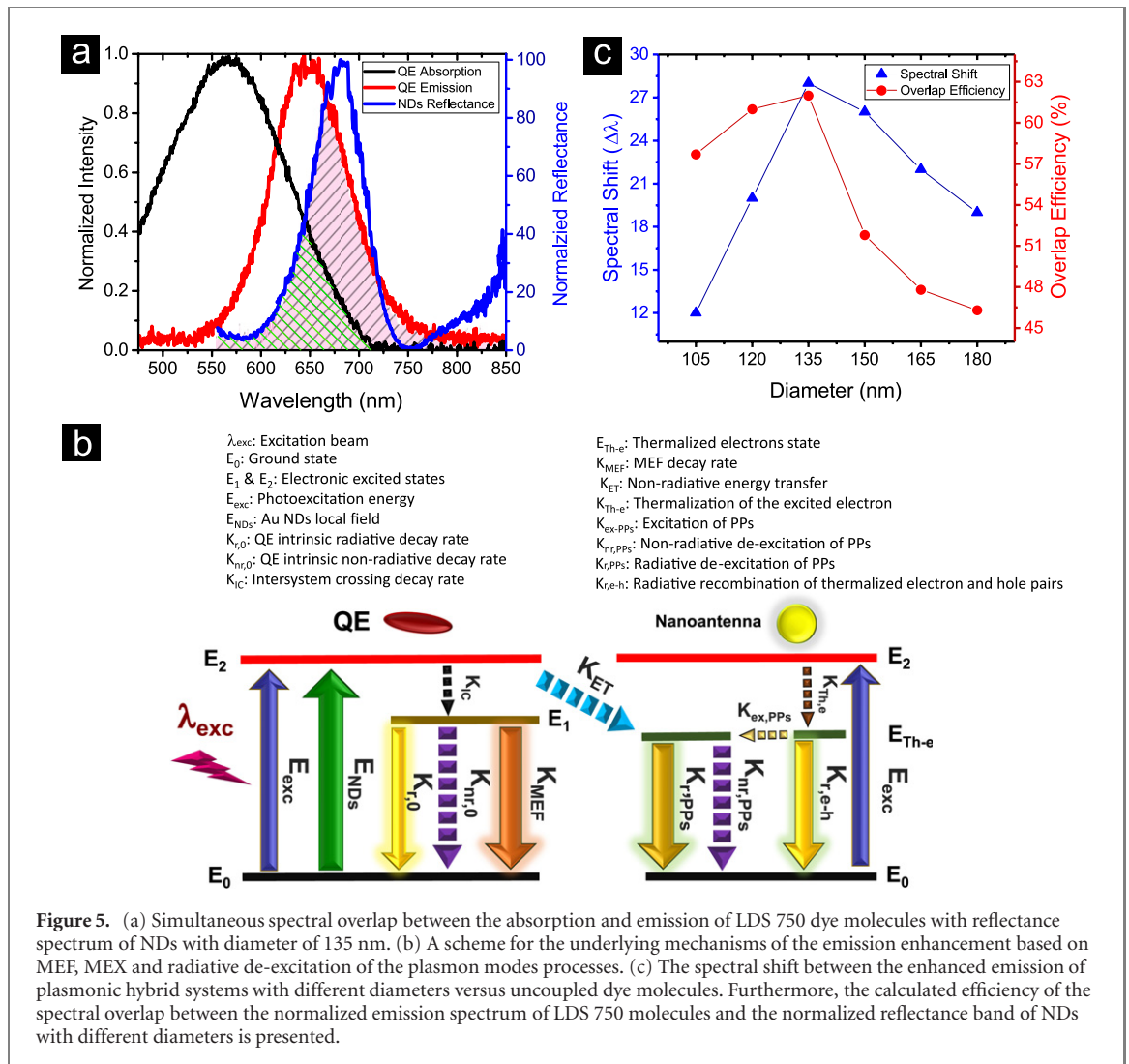
Thus, the mechanisms behind the emission enhancement of an emitter which is located nearby a plasmonic nano-resonator can be explained based on the modification of one or both of these two parameters. For a QE located far from an optical cavity, the Φ_{QE} is defined as follow,

$$\Phi_{QE} = \frac{k_{r,0}}{k_{r,0} + k_{nr,0}} \quad (2)$$

in which the $k_{r,0}$ and $k_{nr,0}$ are intrinsic radiative and non-radiative decay rates, respectively.

The reported several times of magnitude emission rate enhancement in our hybrid exciton–plasmon systems can be explained based on the nano-antenna effect, which leads to the enhancement of the Purcell factor through modifying the Φ_{QE} . This effect, which is so-called metal enhanced fluorescence (MEF), requires spectral overlap between the emission spectrum of the excited QE and the plasmon band of the nano-antenna, as well as, the spatial proximity between the two resonating elements.

The excitation of the dye molecules out of the LSP resonance band of NDs with a 532 nm laser creates oscillating dipoles, which act as small antennas. These oscillating dipoles, at a specific dipole moment orientation [48], may induce collective oscillation of the free electrons in the plasmonic system through non-radiative energy transfer process (K_{ET} in figure 5(b)). This results in a strong oscillating dipole around plasmonic NDs and subsequently local field confinement in the nano-scale range. Embedding LDS 750 molecules in the close vicinity of the nano-antennas can intensify the PDOS. According to the Purcell effect, the plasmonic NDs acting as transmitter nano-antennas outcouple the emission of small oscillating dipoles to the far-field more efficiently [49]. One can consider the interactions between dye molecule dipoles and NDs dipoles almost bidirectional, in which the enhanced local fields around plasmonic nano-resonators

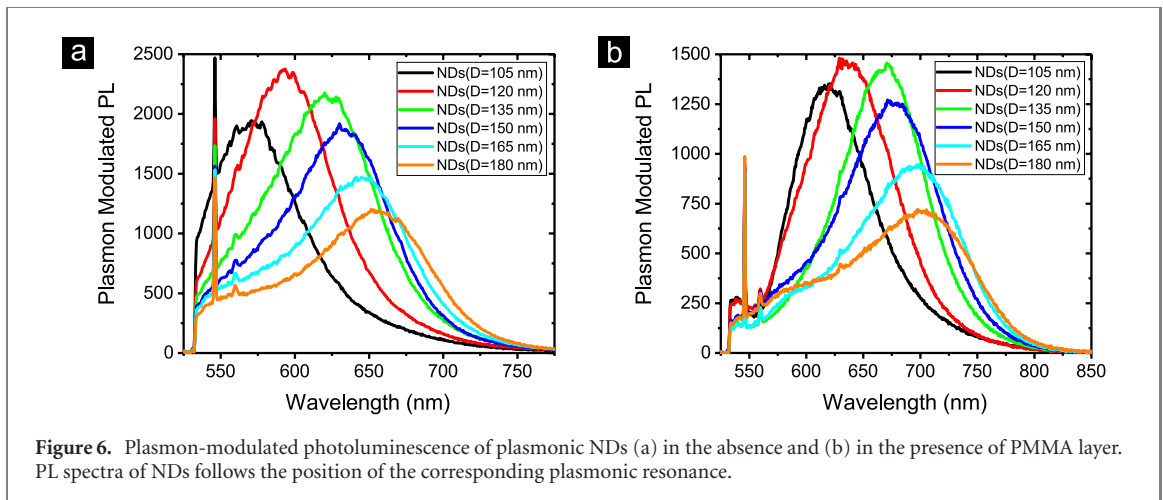


affect the radiative decay rate of the coupled QE. The probability of such bidirectional interaction depends on the efficiency of the spectral and spatial overlaps between two oscillating dipoles of the QE and plasmonic NDs [11, 50]. Considering such bidirectional interaction, the quantum yield of LDS 750 emitter nearby a ND is given by

$$\Phi_{QE-ND} = \frac{k_{r,0} + k_{MEF}}{k_{r,0} + k_{MEF} + k_{nr,0} + k_{ET}}. \quad (3)$$

Such modification in overall radiative decay rate ($k_{r,0} + k_{MEF}$) leads to increase in the quantum yield and consequently a net increase in emission intensity, while the lifetime of the hybrid system decreases [51]. This occurs because most of the excited molecules are knocked down to the ground state through the radiative channels, rather than the non-radiative ones. The relaxed molecules are ready to reabsorb the excitation photons and participate in the photoluminescence process. According to equation (1), this results in the enhancement of the total spontaneous emission rate. This effect can be much more pronounced for a QE with lower quantum yield, since any increase in the radiative decay rate cannot influence the quantum yield if it is already close to unity [52]. The reported low quantum yield values for LDS 750 dye molecules makes it a promising candidate for emission enhancement purposes [53].

The excitation rate (K_{exc}) of a QE with an absorbance in the linear regime (i.e. far from saturation), is directly proportional to the square of the excitation field intensity and molar absorptivity of the QE. In the case of the spectral overlap between the absorption band of QEs and the plasmon band of nano-antennas, the confined electromagnetic fields around nano-antennas act as an extra channel to excite the QE. This effect is the so-called lightning rod effect [54] or metal enhanced excitation (MEX) [19, 51], in which plasmonic structure acts as a receiver nano-antenna, leading to increase the total spontaneous emission rate (K_{em}) by promoting more molecules from the ground state to the excited states. In our designed system, due to the spectral overlap between the absorption band of LDS 750 dye molecules with the plasmon band of the NDs with different diameters, the condition to enhance the excitation rate of the dye molecules is



satisfied. Consequently, in combination with the external excitation field (E_{exc}), the localized electromagnetic fields of NDs (E_{NDs}) act as an extra excitation pathway to enhance the excitation rate of dye molecules. It is easy to distinguish the MEX from MEF, since MEF requires the spectral overlap between the emission band of the QE and the LSPR band of the nano-resonators. Furthermore, in contrast to MEF, this effect will not change the decay rate of the photoexcited molecules, but the peak position of the enhanced PL appears at the same spectral position of the PL signal related to an uncoupled QE.

Figure 5(c) shows the modification of the spectral overlap efficiency between the emission spectrum of LDS 750 dye molecules with the reflectance band of NDs with different diameters. The spectral overlap efficiency is determined as the area of the overlapping region between the NDs reflectance band and the PL spectrum of LDS 750 molecules. It can be also seen that the maximum PL enhancement factor is obtained for NDs with a diameter of 135 nm when the maximum matching occurs between the reflectance band and the emission spectrum of LDS 750 molecules (figure 2(b)). Our reported results prove the correlation between spectral overlap efficiency and the PL spectrum intensification, in which a stronger spectral overlaps result in a higher intensification of the Purcell factor. However, the PL enhancement factor for NDs with larger diameters remains almost the same as that of the smaller NDs, even if the spectral overlap efficiency reduces for NDs with larger diameters. One needs to consider that still larger NDs works as better transmitter antennas and can reradiate or scatter the photons to the far-field in a more efficient way [11]. Additionally, the larger NDs exhibit strong dipole moment and therefore, they can intensify the bi-directional near-field couplings towards radiative decay rate enhancement. On the other hand, according to the MEX effect, the broad reflectance band of NDs with larger diameters provides the required spectral overlap with the absorption spectrum of LDS 750 dye molecules to boost the excitation rate (K_{exc}). Therefore, in our designed system, the larger NDs can operate as an efficient receiver antenna, even though the efficiency of the spectral overlap with the emission spectrum of LDS 750 dye molecules diminishes.

The third mechanism in the spontaneous emission rate enhancement that should be taken into account is the radiative decay of the generated particle plasmons. The PPs can be formed either by the non-radiative energy transfer from the photoexcited gain molecules to the nano-antennas or by the non-radiative recombination of the photoexcited holes in d-band with electrons in SP-band. The specific design of our NDs and photoexcitation of these nano-resonators by using a 2.33 eV excitation source provide the required condition for the radiative decay of the generated PPs [39]. The excitation photons of the laser source promote d-band interband electrons into sp-band, well above the Fermi energy level of the gold. The thermalization of the photoexcited electrons creates inhomogeneous energy distribution of non-equilibrium electrons in the conduction band. The recombination of non-equilibrium electrons with d-band holes leads to PPs generation. These processes are illustrated in the scheme of figure 5(b).

Figure 6 shows the acquired plasmon-modulated photoluminescence of bare plasmonic NDs with various diameters in the absence and the presence of the PMMA layer. The shift of the PL signal to the higher wavelengths is observed, as the diameter of plasmonic nano-antenna increases. Moreover, in general the PL spectrum follows the reflectance band, even if it appears slightly at lower wavelengths with respect to the plasmonic resonance peak. One can expect a stronger PL signal from the NDs with larger diameters or covered with PMMA layer, as they are much more efficient scatters, but the opposite behavior is observed instead. The observed contrast can be explained by the fact that the quantity of the generated PPs can be influenced by the population of the formed non-equilibrium electrons in the photoexcited metal and the number of available PDOS. The localization of the thermalized electrons intensifies where the number of

available PDOS is higher. In other words, as the energy mismatch between the excitation source and reflectance band of NDs ($\Delta E = E_{\text{Excitation}} - E_{\text{plasmon}}$) decreases, the probability for boosting the population of PPs increases. This explains the lower PL intensity of NDs covered by PMMA film than that of NDs exposed to air, even if they function as better scatters in the presence of PMMA layer. In the PL results of larger NDs, one can see that the tail of the spectrum stretches towards the excitation wavelength. This is similar to the PL signal of an unpatterned gold film, resulting from the direct radiative recombination of d-band holes with sp-band electrons [39].

In our hybrid plasmonic system, the number of available PDOS can be intensified by the collective oscillation of the excited free electrons as well as by the resonant interaction between the dipoles of LDS 750 molecules with the confined local field of nano-antennas. In other words, the bi-directional interaction between gain material and plasmonic NDs operates as an extra pathway to amplify the generation of PPs. The generated PPs subsequently decay either radiatively (bright mode PPs) or non-radiatively (dark mode PPs). The radiative damping of the bright mode PPs provides an additional channel for the outcoupling of photons to the far-field in competition to the probable direct radiative recombination of the photoexcited holes with promoted electron above Fermi energy level. Therefore, by considering the plasmon-modulated PL of gold nanostructures (k_{PPs}) as an additional gateway to modify the spontaneous decay rate, the $\Phi_{\text{QE-ND}}$ of an emitter nearby a ND antenna can be rewritten as follows

$$\Phi_{\text{QE-ND}} = \frac{k_{r,0} + k_{\text{MEF}} + k_{\text{PPs}}}{k_{r,0} + k_{\text{MEF}} + k_{\text{PPs}} + k_{\text{nr},0} + k_{\text{ET}}}. \quad (4)$$

As is evident in figure 2(a), the emission peak of the enhanced PL in plasmonic hybrid systems is mismatched compared to the emission peak of the reference dye molecules. Figure 5(c) shows the red-shift of the enhanced PL peak for different diameters of plasmonic nano-antennas. Notably, the red-shift of the intensified emission spectrum goes up, as the diameter of nano-antennas increases, and it reaches the maximum for NDs with 135 nm diameter. After that it goes down for NDs with larger diameters. The observed red-shift in the PL spectra is considered as the overall evidence for the manifestation of the plasmon-modulated PL of the plasmonic nano-antennas in the enhanced PL spectra of the hybrid system. The bright mode PPs which decay radiatively track the reflectance band of NDs. Overall, the observed enhanced emission is the superposition of this process with MEF and MEX processes.

The designed hybrid exciton–plasmon system operates as a radiating antenna to outcouple efficiently the bright mode PPs to the far-field. An efficient coupling between oscillating dipoles of the photoexcited dye molecules and plasmonic antenna can induce stronger collective oscillation of the plasmonic dipoles, providing larger local density of optical states [55–57]. According Fermi’s golden rule, due to the larger number of available PDOS, the non-equilibrium electrons have a higher probability to excite PPs and subsequently the probability for the radiative decay of the PPs increases. This leads to the achieved maximum PL enhancement and the maximum PL red-shift for 135 nm NDs, in which the most efficient spectral overlap occurs. On the other hand, the reported PL red-shift for NDs with diameters larger than 135 nm is pronounced compared to smaller ones. In fact, larger NDs with stronger confined local field can act as better radiating antennas to outcouple PPs. However, by increasing diameter the performance of nano-antennas for radiating out the PPs is hindered due to the diminishing of the spectral overlap efficiency and increasing energy mismatch of ΔE . Hence, the observed intensified PL of larger NDs is attributed partially to MEF effect and MEX effect.

4. Conclusion

To summarize, we explored different underlying mechanisms related to the observed emission enhancement in our designed plasmonic hybrid systems. The systems are engineered to exploit the enhanced local field of the lithographically fabricated plasmonic NDs in the direction of both radiative decay rate and excitation rate enhancement of the QEs. We show that the simultaneous spectral overlap of a nano-antenna’s resonance band with the absorption and emission spectra of an emitter leads to enhanced emission from QEs with low quantum efficiency. The overall evidence for the manifestation of the PL enhancement via bidirectional near-field coupling is the reduction in the decay time of the excited molecule, due to the modification of the radiative and non-radiative decay rates. The measured plasmon-modulated PL signals of NDs in the presence and the absence of PMMA layer are established from polarizing nanostructures by highly localized d-hole photoexcitation. However, owing to the elaborated design of the hybrid systems, beside the non-radiative recombination of the photoexcited d-band holes with non-equilibrium electrons, the near-field coupling between the photoexcited dye molecules and NDs functions as the second pathway to imply PPs in NDs. This additional pathway leads to the amplification and more efficient outcoupling of the plasmon-modulated PL in hybrid plasmonic systems with respect to the bare plasmonic systems. We

show that in plasmonic hybrid systems with an efficient spectral overlap and therefore larger availability of PDOS this amplification process is boosted. Our theoretical and experimental analyses show that the contribution of the outcoupled PPs in the enhancement of the radiative decay rate process manifests itself as a red-shift in the enhanced emission spectrum peak of the hybrid systems as compared to that of the uncoupled dye molecules. These results provide crucial knowledge to engineer hybrid exciton–plasmon systems to unlock promising applications of nanophotonic devices.

5. Methods

5.1. Simulation

Simulations were conducted utilizing the FDTD method, implemented with the aid of a commercial software package (Lumerical FDTD Solutions). Gold nanostructures with various diameters are modeled with a frequency dependent dielectric function taken from Johnson and Christy [58], while 5 nm Al_2O_3 spacer is simulated using the reported data in reference [59]. For the case in which the surrounding environment of NDs was considered as PMMA, the dielectric constant data is adopted from reference [60]. In local field simulation, the incident field is a transverse electromagnetic plane wave with electric and magnetic fields in X and Y directions, respectively, while wave propagates in Z direction. Along with this excitation, electric dipole resonators are formed in X direction. The normalized field profiles were calculated at the maximum reflectance wavelength of the NDs and plotted in XY cross-section plane. In reflectance simulations, the reflected signal is collected from the structure surface, as the injected beam of the source is considered to propagate in the Z direction with a normal incident.

5.2. Fabrication

The Si/SiO₂ are used as substrates for fabricating plasmonic NDs as a right candidate to avoid charging effects during the EBL process. The thickness of SiO₂ on silicon substrates was 280 nm, which is deposited by plasma-enhanced chemical vapor deposition (PECVD) method to eliminate any possible polar and nonpolar impurities, the SiO₂/Si substrate are sonicated for 20 min in acetone and then soaked and rinsed with fresh acetone and IPA solvent, respectively. The positive PMMA A4 photoresist (950 K molecular weight) from microchem corp. is spin-coated at 3000 rpm for 40 s on cleaned substrate to create a layer with the thickness of approximately 200 nm. After that the spin-coated resist is baked for 90 s at 180 °C. The NDs with varied diameters from 105 to 180 nm and the constant period of 400 nm are fabricated using standard EBL method. The coated sample with PMMA is exposed to a dose of 2000 pC cm⁻² under E-beam with an accelerating voltage of 20 kV to form NDs. The exposed samples were developed with 1:1 MIBK/IPA developer for 1 min and then they are kept in IPA as the stopper solvent for 30 s. Then, the developed samples are directly blown to be dried using N₂. The metallization process is completed by depositing 70 nm thick gold layer using an E-beam evaporator machine at the constant rate of 0.5 Å s⁻¹ and a vacuum pressure of 1 × 10⁻⁶ mbar. During the entire deposition process, the sample chamber is cooled down below room temperature with the continuous flow of cold water. The nanostructures appeared after the lift-off process, by soaking the samples for 24 h in acetone. The 5 nm spacer is deposited on top of NDs using atomic layer deposition method to create a precise and smooth layer of Al₂O₃. LDS 750 dye molecules are dissolved in PMMA A2 (950 K molecular weight), provided by EM Resist LTD, with a mass percent concentration of 0.01% (see supplementary material, section 3 for further details). To avoid the aggregation of the incorporated dye molecules in PMMA, the prepared samples are sonicated at low temperature for 30 min. Moreover, to homogenize the prepared samples, the dye-PMMA samples are stirred for at least 90 s with a vortex mixer operating at 3000 rpm. Then the active PMMA layer is spin-coated on top of NDs coated with Al₂O₃ at 4000 rpm for 40 s. To avoid any change in the chemical and optical properties of the incorporated LDS 750 dye molecules in PMMA, instead of baking, the samples are left overnight to evaporate the anisole solvent at room temperature. This process leads to LDS 750 molecules embedded homogeneously in the PMMA polymer.

5.3. Characterization

Reflectance, PL, fluorescent lifetime and FLIM measurements of Au nanostructure are performed on a multi-functional WITec alpha300C confocal Raman microscopy system. The reflectance bands are acquired using an ultrahigh throughput spectrometer equipped to 150 lines/mm grating and detected using a thermoelectrically cooled, back-illuminated CCD camera. For reflectance measurements the samples are illuminated by highly bright and stable broadband light (LDLS EQ-99X) through a Zeiss EC 'Epiplan' DIC, 20× air objective (NA = 0.4, WD = 3.0 mm) and the reflected signal through the samples surfaces are detected by ultra-high throughput spectrometer, equipped with 150 lines/mm grating and a TE-cooled CCD (Andor DV 401-BV-351) camera. The reflectance spectra (R_{fl}) are calculated according to the

following formula

$$\text{Rfl} = \frac{I_{\text{Rfl-NDs}} - I_{\text{sub}}}{I_{\text{source}} - I_{\text{BG}}} \quad (5)$$

where $I_{\text{Rfl-NDs}}$ is the collected reflection spectrum of the nanostructures and I_{source} is the acquired spectrum of the broadband light source, which is measured using a perfect reflector. I_{sub} is the substrate reflection, acquired from the un-patterned area of the Si/SiO₂ substrate and I_{BG} stands for the background counts, acquired by the used system.

The transmittance spectra (Tra) for NDs on sapphire substrate are calculated as follows

$$\text{Tra} = \frac{I_{\text{Tra-NDs}} - I_{\text{BG}}}{I_{\text{sub}} - I_{\text{BG}}} \quad (6)$$

where $I_{\text{Tra-NDs}}$ is the collected transmission spectrum of the NDs on sapphire and here I_{sub} stands for the substrate transmission, acquired from the un-patterned area of the sapphire substrate.

The photoluminescence spectra of the control and main samples are acquired utilizing VIS-NIR Flame detector (350–1000 nm) provided by Ocean Optics with an integration time of 300 ms. The samples are excited with 532 nm CW laser and the PL signals are guided to the detector through a 50× Zeiss EC ‘Epiplan’ DIC objective, (NA = 0.75, WD = 1.0 mm). The background counts are subtracted from the measured PL spectra. To calculate the PL enhanced factor, the acquired results are normalized to the PL signal which is acquired from an un-patterned area of the spin-coated substrate with gain-doped PMMA. For power-depended PL experiments the laser power is varied in the range of 10 to 100 mW, which is measured inside the microscope, right before impinging to the objective.

For lifetime measurements the samples are excited using a 532 nm pulsed laser beam. To generate the excitation pulses in the visible range (420–700 nm), the output of the ps super-continuum Fianium laser is connected to an acoustic optical tunable filter. The photons of the excited sample are collected using the 50× objective and detected by the single-photon avalanche diode (SPAD) detectors, provided by Picoquant, feature an extremely high photon detection efficiency up to 70%, operating in the range of 400 nm to 1100 nm. The acquired time-correlated single-photon counting data (TCSPC) is processed by a time to digital converter (TDC) module, provided by Picoquant and the results are analyzed by SymPhoTime 64 software.

To perform FLIM measurement, a motorized stage with a step size of 100 nm and reproducibility better than 0.01% is used to scan the selected area of the samples. The acquired signal is collected using 50× objective and detected by avalanche photodiode detector, provided by MPD company, operating in the spectral range 400–1050 nm and with optimized timing resolution down to 50 ps. Collected photons are processed by a TCSPC module, provided by WITec, and the results are analyzed by microscope software.

Acknowledgments

We acknowledge the financial support of Academy of Finland Flagship Programme (PREIN) (320165) and Academy of Finland Competitive funding to strengthen university research profiles (301820).

ORCID iDs

Alireza R Rashed  <https://orcid.org/0000-0002-3838-8966>

Mohsin Habib  <https://orcid.org/0000-0002-6109-9468>

Humeyra Caglayan  <https://orcid.org/0000-0002-0656-614X>

References

- [1] Senellart P, Solomon G and White A 2017 *Nat. Nanotechnol.* **12** 1026
- [2] Hertel F, Li S, Chen M, Pott L, Mehta S and Zhang J 2020 *ACS Chem. Biol.* **15** 33–8
- [3] Tame M S, McEnery K R, Özdemir Ş K, Lee J, Maier S A and Kim M S 2013 *Nat. Phys.* **9** 329–40
- [4] Aharonovich I, Englund D and Toth M 2016 *Nat. Photon.* **10** 631
- [5] Hakala T, Rekola H, Vakevainen A, Martikainen J P, Necada M, Moilanen A and Torma P 2017 *Nat. Commun.* **8** 13687
- [6] Dhawan A R *et al* 2020 *Light: Sci. Appl.* **9** 33
- [7] Emam A N, Mansour A S, Mohamed M B and Mohamed G G 2020 *Plasmonic Hybrid Nanocomposites for Plasmon-Enhanced Fluorescence and Their Biomedical Applications* (Berlin: Springer)
- [8] Ghopry S A, Alamri M, Goul R, Cook B, Sadeghi S, Gutha R, Sakidja R and Wu J Z 2020 *ACS Appl. Nano Mater.* **3** 2354–63
- [9] Norville C A, Smith K Z and Dawson J M 2020 *Appl. Opt.* **59** 2308–18
- [10] Yarak M T, Rezaei S D and Tan Y N 2020 *Phys. Chem. Chem. Phys.* **22** 5673–87
- [11] Viste P, Plain J, Jaffiol R, Vial A, Adam P M and Royer P 2010 *ACS Nano* **4** 759–64

- [12] Rashed A R, De Luca A, Dhama R, Hosseinzadeh A, Infusino M, El Kabbash M, Ravaine S, Bartolino R and Strangi G 2015 *RSC Adv.* **5** 53245–54
- [13] Matsuda K, Ito Y and Kanemitsu Y 2008 *Appl. Phys. Lett.* **92** 211911
- [14] Anger P, Bharadwaj P and Novotny L 2006 *Phys. Rev. Lett.* **96** 113002
- [15] Shahbazyan T V 2013 *Nano Lett.* **13** 194–8
- [16] Hoang T B, Akselrod G M, Argyropoulos C, Huang J, Smith D R and Mikkelsen M H 2015 *Nat. Commun.* **6** 7788
- [17] Russell K J, Liu T-L, Cui S and Hu E L 2012 *Nat. Photon.* **6** 459–62
- [18] Berini P and De Leon I 2012 *Nat. Photon.* **6** 16
- [19] Lakowicz J R 2005 *Anal. Biochem.* **337** 171–94
- [20] Nguyen M, Kim S, Tran T T, Xu Z-Q, Kianinia M, Toth M and Aharonovich I 2018 *Nanoscale* **10** 2267–74
- [21] Zalogina A S, Savelev R S, Ushakova E V, Zograf G P, Komissarenko F E, Milichko V A, Makarov S V, Zuev D A and Shadrivov I V 2018 *Nanoscale* **10** 8721–7
- [22] Schniepp H and Sandoghdar V 2002 *Phys. Rev. Lett.* **89** 257403
- [23] Russell K J, Liu T-L, Cui S and Hu E L 2012 *Nat. Photon.* **6** 459–62
- [24] Pelton M 2015 *Nat. Photon.* **9** 427
- [25] Wenger J, Gerard D, Dintinger J, Mahboub O, Bonod N, Popov E, Ebbesen T W and Rigneault H 2008 *Opt. Express* **16** 3008–20
- [26] Anger P, Bharadwaj P and Novotny L 2006 *Phys. Rev. Lett.* **96** 113002
- [27] Lakowicz J R and Fu Y 2009 *Laser Photon. Rev.* **3** 221–32
- [28] Ureña E B, Kreuzer M P, Itzhakov S, Rigneault H, Quidant R, Oron D and Wenger J 2012 *Adv. Mater.* **24** OP314–20
- [29] Pompa P P, Martiradonna L, Torre A D, Sala F D, Manna L, De Vittorio M, Calabi F, Cingolani R and Rinaldi R 2006 *Nat. Nanotechnol.* **1** 126–30
- [30] Shahbazyan T V, Perakis I E and Bigot J-Y 1998 *Phys. Rev. Lett.* **81** 3120
- [31] Ngoc L L T, Wiedemair J, van den Berg A and Carlen E T 2015 *Opt. Express* **23** 5547–64
- [32] Boyd G T, Yu Z H and Shen Y R 1986 *Phys. Rev. B* **33** 7923
- [33] Apell P, Monreal R and Lundqvist S 1988 *Phys. Scr.* **38** 174
- [34] Varnavski O P, Mohamed M B, El-Sayed M A and Goodson T 2003 *J. Phys. Chem. B* **107** 3101–4
- [35] Mohamed M B, Volkov V, Link S and El-Sayed M A 2000 *Chem. Phys. Lett.* **317** 517–23
- [36] Shahbazyan T V 2013 *Nano Lett.* **13** 194–8
- [37] Dulkeith E, Niedereichholz T, Klar T, Feldmann J, Von Plessen G, Gittins D, Mayya K and Caruso F 2004 *Phys. Rev. B* **70** 205424
- [38] Tcherniak A, Dominguez-Medina S, Chang W-S, Swanglap P, Slaughter L S, Landes C F and Link S 2011 *J. Phys. Chem. C* **115** 15938–49
- [39] Hu H, Duan H, Yang J K W and Shen Z X 2012 *ACS Nano* **6** 10147–55
- [40] Ringler M, Schwemer A, Wunderlich M, Nichtl A, Kurzinger K, Klar T and Feldmann J 2008 *Phys. Rev. Lett.* **100** 203002
- [41] Goffard J, Gerard D, Miska P, Baudrion A L, Deturche R and Plain J 2013 *Sci. Rep.* **3** 2672
- [42] Zhao J, Cheng Y, Shen H, Hui Y Y, Wen T, Chang H C, Gong Q and Lu G 2018 *Sci. Rep.* **8** 3605
- [43] ElKabbash M et al 2019 *Phys. Rev. Lett.* **122** 203901
- [44] Udayan S, Sebastian M, Vijesh K, Nampoori V and Thomas S 2018 *J. Lumin.* **194** 428–32
- [45] Fan R, Xia Y and Chen D 2008 *Opt. Express* **16** 9804–10
- [46] Rodríguez-Fernández J, Pastoriza-Santos I, Pérez-Juste J, García de Abajo F J and Liz-Marzán L M 2007 *J. Phys. Chem. C* **111** 13361–6
- [47] Kim J, Lee M, Yang J-H and Choy J-H 2000 *J. Phys. Chem. A* **104** 1388–92
- [48] Dulkeith E, Ringler M, Klar T A, Feldmann J, Muñoz Javier A and Parak W J 2005 *Nano Lett.* **5** 585–9
- [49] Hoang T B, Akselrod G M, Argyropoulos C, Huang J, Smith D R and Mikkelsen M H 2015 *Nat. Commun.* **6** 7788
- [50] Singh M P and Strouse G F 2010 *J. Am. Chem. Soc.* **132** 9383–91
- [51] Lakowicz J R 2001 *Anal. Biochem.* **298** 1
- [52] Punj D, Mivelle M, Moparthy S B, Van Zanten T S, Rigneault H, Van Hulst N F, García-Parajó M F and Wenger J 2013 *Nat. Nanotechnol.* **8** 512
- [53] Liu C, Eliseeva S V, Luo T-Y, Muldoon P F, Petoud S and Rosi N L 2018 *Chem. Sci.* **9** 8099–102
- [54] Aktsipetrov O, Baranova I, Mishina E and Petukhov A 1984 *JETP Lett.* **40** 1012–5
- [55] Pelton M 2015 *Nat. Photon.* **9** 427–35
- [56] Nguyen M, Kim S, Tran T T, Xu Z-Q, Kianinia M, Toth M and Aharonovich I 2018 *Nanoscale* **10** 2267–74
- [57] Shahbazyan T V 2016 *Phys. Rev. Lett.* **117** 207401
- [58] Johnson P B and Christy R W 1972 *Phys. Rev. B* **6** 4370
- [59] Boidin R, Halenkovič T, Nazabal V, Beneš L and Němec P 2016 *Ceram. Int.* **42** 1177–82
- [60] Beadie G, Brindza M, Flynn R A, Rosenberg A and Shirk J S 2015 *Appl. Opt.* **54** F139–43